THE JOURNAL OF PHYSICAL CHEMISTRY C

Article

pubs.acs.org/JPCC

Assembling of Silicon Nanoflowers with Significantly Enhanced Second Harmonic Generation Using Silicon Nanospheres Fabricated by Femtosecond Laser Ablation

Chang-Qing Li,[†] Cheng-Yun Zhang,[†] Zao-Shan Huang,[†] Xian-Feng Li,[†] Qiao-Feng Dai,[†] Sheng Lan,*[,†] and Shao-Long Tie[‡]

[†]Laboratory of Nanophotonic Functional Materials and Devices, School of Information and Optoelectronic Science and Engineering, South China Normal University, Guangzhou 510006, People's Republic of China

[‡]School of Chemistry and Environment, South China Normal University, Guangzhou 510006, People's Republic of China

ABSTRACT: Silicon (Si) nanospheres (NSs) with diameters ranging from about 10 to 100 nm were fabricated by using femtosecond (fs) laser ablation of a silicon wafer immersed in deionized water. Si nanoflowers (NFs) looking like snowflakes were assembled by dropping and drying the colloid solution on a glass slide. Transmission electron microscope observation revealed that Si NFs were composed of self-assembled Si NSs with different sizes. The nonlinear optical responses of both single Si NSs and Si NFs were examined by using a focused fs laser at ∼800 nm. While only second harmonic generation (SHG) with weak intensity was observed for single Si NSs, a significant enhancement in SHG was found for Si NFs. More interestingly, both the Stokes and anti-Stokes components of the Raman scattering of the SH were also revealed in the nonlinear response spectra of Si NFs, possibly due to the large enhancement in SHG. The electric field distributions were numerically simulated by using the finite-difference time-domain technique for single Si NSs and corresponding aggregates composed of seven closely packed NSs at the wavelengths of both the fundamental light and the SH. It was revealed that the significant enhancement in electric field achieved in the aggregates of Si NSs is responsible for the strong SHG observed in Si NFs.

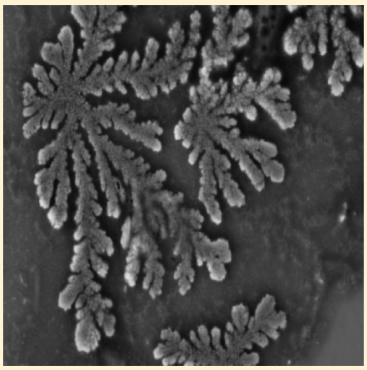

1. INTRODUCTION

As an important semiconductor, silicon (Si) has been widely applied in the fabrication of electronic devices in the past century.[1] Unfortunately, the low emission efficiency originating from its indirect bandgap has severely hampered its applications in making optical devices. In the past two decades, much effort has been devoted to the improvement of the optical properties of Si. It has been demonstrated that a significant improvement in emission efficiency can be achieved in porous Si or Si nanocrystals.[2−6] Stimulated by this improvement, various chemical[7−12] and physical[13−23] methods have been proposed to synthesize or fabricate Si nanoparticles (NPs) with diameters ranging from a few to several tens of nanometers. One of the motivations is the use of Si NPs, which is highly biocompatible, as imaging agents in the field of biophotonics. As compared to colloidal semiconductor quantum dots such as CdS and CdSe, the high compatibility and low toxicity of Si NPs make them quite attractive for bioimaging application. In fact, the femtosecond (fs) laser generated silicon NPs have already shown promising properties in the biophotonics and bioimaging field as well as their highly biocompatibility with respect to heavy metal semiconductor materials.[24,25] Among various chemical and physical methods, pulsed laser ablation of Si wafer[13−23] has emerged as a simple and effective tool to obtain Si NPs with controllable size. It has been shown that the size of Si NPs can be easily controlled by varying the ablation parameters such as pulse duration,[21] laser fluence,[16] and irradiation time.[23] In order to avoid the oxidation occurring on the surfaces of Si NPs, the laser ablation is usually carried out in ethanol.[21]

From the viewpoint of practical application, Si NPs with small size and high luminescent efficiency are highly desirable. For this reason, Si NPs with sizes of a few nanometers have been the focus of many studies. Very recently, it was found that Si nanospheres (NSs) with diameters in the range of 100−200 nm exhibited an intriguing scattering property which is referred to as "magnetic light".[26−28] Based on theoretical analysis and experimental observation, it was revealed that the scattering in such Si NSs with appropriate diameters is dominated by magnetic dipole scattering rather than the conventional electric dipole one. The underlying physical mechanism is the formation of a circular electric field inside the NS which induces a strong oscillation of the magnetic dipole. The Si NSs with such scattering property are considered to be promising building blocks for constructing metamaterials in the near-

Received: September 4, 2013
Revised: October 16, 2013

   dx.doi.org/10.1021/jp408865p | J. Phys. Chem. C XXXX, XXX, XXX−XXX

infrared and visible light regions where most metallic nanostructures fail to work.

So far, most studies in this field concentrate on the linear optical properties of Si NPs such as scattering and luminescence under single photon excitation. In comparison, less attention has been paid to their nonlinear optical properties such as second harmonic generation (SHG) and two-photon-induced photoluminescence (TPL). Previously, the SHG and TPL of very small Si NPs (about 1 nm) have been investigated.[29,30] It was found that very strong SHG could be generated by such Si NPs although SHG is not allowed in bulk Si due to its centrosymmetry. In addition, efficient TPL was observed for such Si NPs which exhibit strong direct-like oscillator strength.[11] However, the nonlinear optical properties of Si NPs with diameters in the range of about 10−100 nm remain unexplored. The scattering peaks of such Si NPs appear in the violet and blue light regions. A significant enhancement in the electric field is expected for such Si NPs at the wavelength of the SH (~400 nm) if they are excited with a fs laser at ~800 nm. Therefore, it is quite interesting to investigate the fabrication and nonlinear optical properties of such Si NPs and the related aggregates.

In this article, we report on the fabrication of Si nanospheres (NSs) whose diameters are in the range of about 10−100 nm by using fs laser ablation of Si wafer in deionized water and the assembling of Si nanoflowers (NFs) by using the as-prepared Si NSs. The morphologies of Si NSs and NFs were characterized by scanning electron microscopy (SEM) and transmission electron microscopy (TEM). The linear optical properties of Si NSs were examined by scattering and luminescence spectra measurements. More importantly, the nonlinear optical responses of Si NSs and NFs were investigated by exciting them with a focused fs laser beam. While only SHG with weak intensity was observed for Si NSs, a significant enhancement in SHG as well as the Raman scattering of the SH was found for Si NFs. We explain the experimental observations by comparing the electric field distributions in both single NSs and the related aggregates calculated by using the finite-difference time-domain (FDTD) technique.

2. EXPERIMENTAL SECTION

We employed fs laser ablation to fabricate Si NSs with diameters ranging from about 10 to 100 nm. In experiments, a 800 nm fs laser light delivered by a fs amplifier (Legend Elite, Coherent) with a pulse duration of 90 fs and a repetition rate of 1 kHz was focused on the surface of a Si wafer, which was immersed in deionized water, by using a lens with a focusing length of 150 mm. The lateral dimension of the cuvette we used was 1 cm × 1 cm, and the volume of water was 1.0 mL. The diameter of the laser beam on the surface of the Si wafer was estimated to be ~40 μm. The size of the fabricated Si NSs was controlled by adjusting the fluence and scanning speed of the fs laser light. While the ablation time was fixed at 2 h, two laser fluences (0.14 and 0.24 J/cm^2) and two scanning speeds (0.5 and 1.0 mm/s) were employed in the ablation of the Si wafer. It was found that the influence of the scanning speed on the size of the generated Si NSs was quite small, and Si NSs with a large size distribution were obtained. Once the ablation was completed, the aqueous solution containing Si NSs was centrifuged with a speed of 12 000 rpm to separate NSs with small and large sizes which are distributed in the upper and lower parts of the aqueous solution. Based on SEM and TEM observations, the diameters of small NSs were less than 10 nm. The large NSs with diameters ranging from 10 to more than 100 nm were used for the assembling of Si NFs. The emission spectra of Si NSs with small and large sizes were measured by using a luminescence spectrometer (F-4600, Hitachi) with an excitation wavelength at 270 nm. For morphology and optical characterizations, the aqueous solution of Si NSs was dropped and dried on a glass slide or a Si substrate. The assembling of Si NFs was completed after the evaporation of water. The morphologies of single NSs and NFs were examined by SEM (Ultra55, Zeiss) and TEM (JEM-2100HR, JEOL) observations. Meanwhile, the nonlinear optical properties were characterized by using an inverted microscope (Axio Observer A1, Zeiss) equipped with a spectrometer (SR-500i-B1, Andor) and a coupled-charge device (DU970N, Andor). The fs laser light was focused on NSs and NFs by using the 100× objective lens of the microscope, and the generated nonlinear optical signals were collected by using the same objective lens and delivered to the spectrometer for analysis. The diameter of the excitation spot was estimated to be about 1.0 μm.

3. RESULTS AND DISCUSSION

3.1. Morphologies and Linear Optical Properties of Si NSs and NFs. The morphologies of the as-prepared Si NSs and NFs were examined by SEM observation. A typical example for Si NSs is shown in Figure 1 where single Si NSs with diameters ranging from about 10 to 100 nm are clearly identified. These Si NSs were found at areas where the densities of NPs are small. At places where the densities of NPs are large, we observed the formation of Si NFs, as shown in Figure 2. We also performed chemical analysis for Si NFs assembled on a silicon substrate; only Si and O were found (see Figure 2g). Thus, the presence of other impurities in the solution can be excluded.

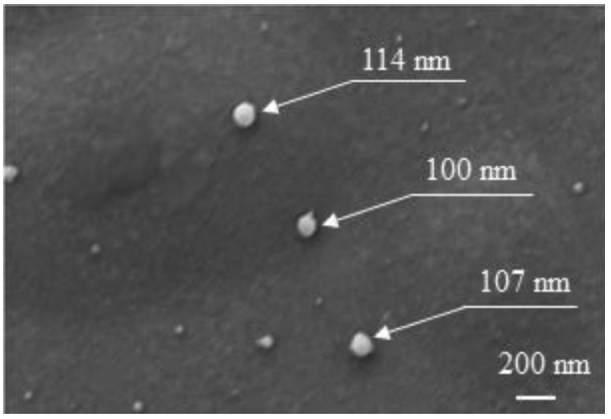

Figure 1. SEM image for single Si NSs obtained by the fs laser ablation of a Si wafer in deionized water. The laser fluence, scanning speed, and ablation time were chosen to be 0.14 J/cm^2, 1.0 mm/s, and 2 h, respectively.

In order to confirm that Si NFs observed in the SEM observations are composed of Si NSs with different sizes, some Si NFs were examined by TEM measurements, and a typical example is presented in Figure 3a. It can be clearly seen that the Si NF really consists of Si NSs with different diameters ranging from about 10 to 100 nm. The Si NSs are closely packed with quite narrow gaps in between them. It will be shown in the following that the assembling of Si NSs in this form leads to a strong electric field in the gaps, resulting in a significant

dx.doi.org/10.1021/jp408865p | J. Phys. Chem. C XXXX, XXX, XXX−XXX

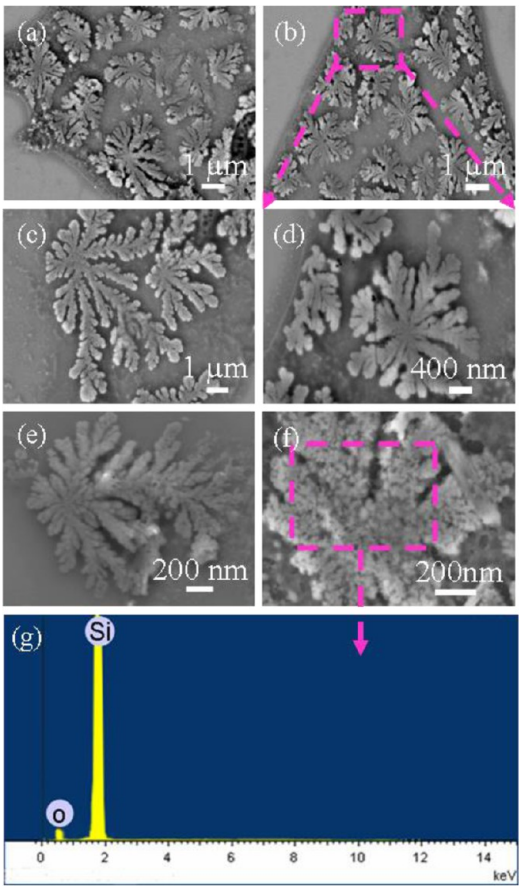

Figure 2. SEM images for Si NFs self-assembled by Si NSs fabricated by fs laser ablation. The laser fluence, scanning speed, and ablation time were chosen to be 0.14 J/cm^2, 0.5 mm/s, and 2 h, respectively. (a, b) Two areas where many Si NFs were observed. (c–e) Magnified images for Si NFs showing the detailed structures. (f) Si NF on which the chemical analysis (g) was performed.

enhancement in SHG as compared to single Si NSs. In addition to the arrangement of Si NSs in the Si NF, the diffraction pattern measured for a single Si NS indicates the single crystallinity of the fabricated Si NSs, as shown in Figure 3b.

The emission spectra of small- and large-sized Si NSs suspended in water was characterized by using single photon excitation at 270 nm. A typical example is shown in Figure 4. For small-sized Si NSs, a strong emission peak was observed at ~300 nm while a weak one was found at ~440 nm. In comparison, the emission spectrum for large-sized Si NSs was dominated by the broad emission peak at ~440 nm, possibly originating from the electronic transitions between the energy levels in Si/SiO_2 quantum dots, including defect levels.

3.2. Nonlinear Optical Properties of Single Si NSs. Before discussing the nonlinear optical properties of Si NFs, we first examined the nonlinear optical responses of single Si NSs which are the building blocks of Si NFs. For this purpose, we studied a Si NS whose diameter was measured to be ~118 nm, as shown in the inset of Figure 5a. Figure 5a presents the scattering spectrum of the Si NS obtained by using dark-field microscope. A resonant peak was found to appear at ~475 nm.

The excitation-intensity-dependent nonlinear response spectrum of the Si NS obtained at an excitation wavelength of 800 nm is shown in Figure 5b. At each excitation intensity, only a peak at 400 nm was observed, and it was attributed to the SHG

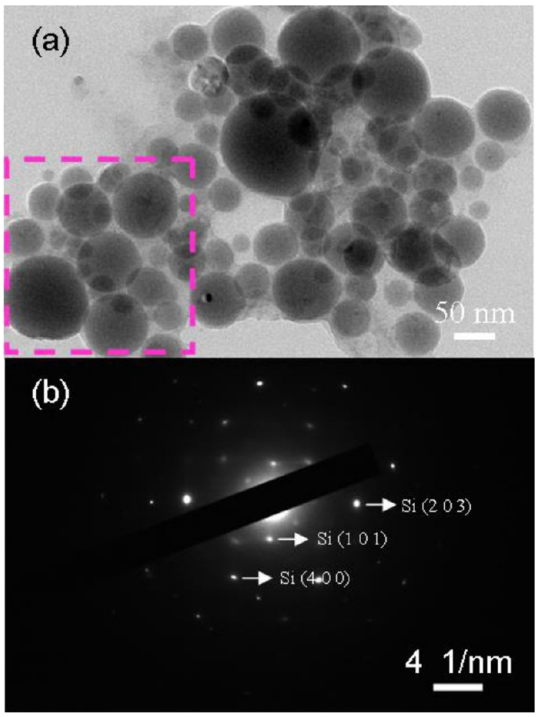

Figure 3. (a) TEM image of a typical Si NF. (b) Diffraction pattern observed for a single Si NS.

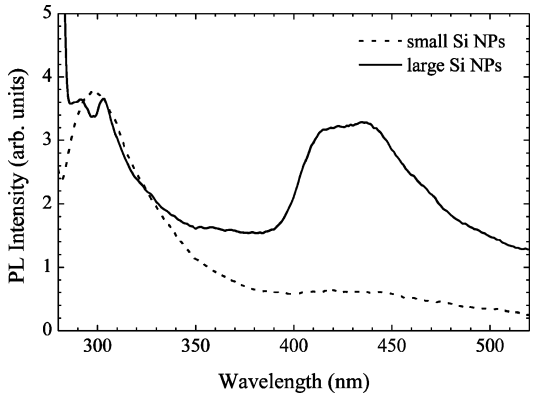

Figure 4. Emission spectra measured for small- and large-sized Si NSs under single photon excitation at 270 nm.

because its wavelength was shifted accordingly when we tuned the excitation wavelength around 800 nm. In addition, a slope of ~1.81 was derived from the excitation-intensity-dependent SHG, as shown in Figure 5c. It is in good agreement with the second-order nature of SHG. Since the SHG intensity was very weak, a 10× gain was used when measuring the nonlinear response spectra.

3.3. Nonlinear Optical Properties of Si NFs: Significant Enhancement in SHG. The nonlinear response spectra of several Si NFs were characterized by exciting them with focused fs laser light. Figure 6 shows the evolution of nonlinear response spectrum with increasing excitation intensity measured for three different Si NFs. The excitation wavelengths for them were intentionally chosen to be different. In each case, one can find a strong SHG located at half of the excitation wavelength. However, it is noticed that the spectra shown in Figure 6a appear to be different from those shown in Figures 6b and 6c. In Figure 6a, one can see two peaks in the spectra. The

dx.doi.org/10.1021/jp408865p | J. Phys. Chem. C XXXX, XXX, XXX–XXX

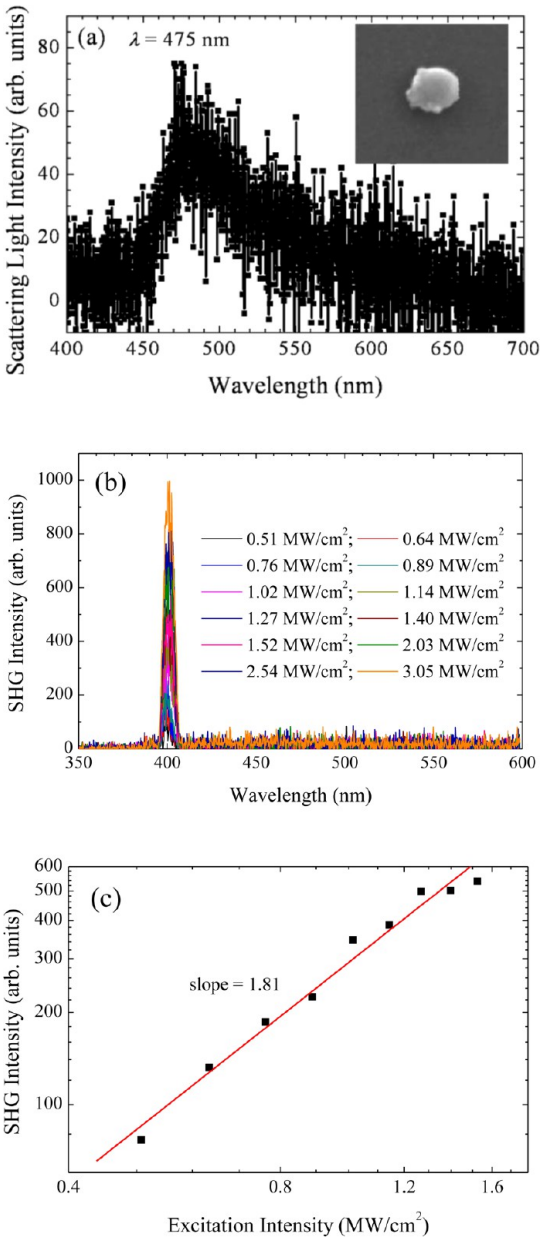

Figure 5. (a) Scattering spectrum measured for a single Si NS with a diameter of ∼118 nm. The inset shows the SEM image of the Si NS. (b) Excitation-intensity-dependent nonlinear response spectrum measured for the same Si NS. (c) Excitation-intensity-dependent SHG from which a slope of ∼1.81 was derived.

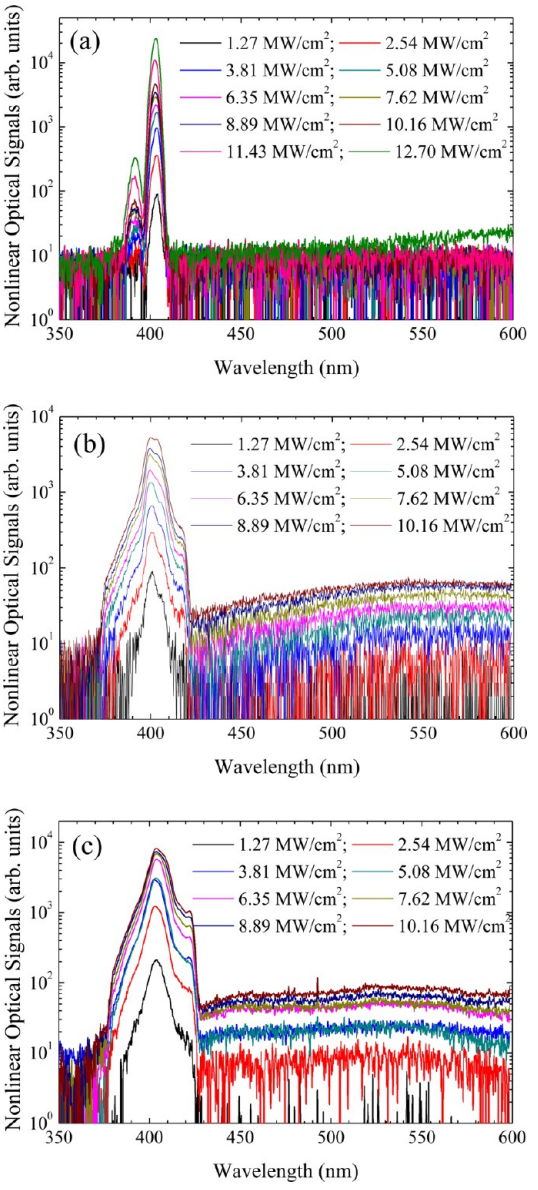

Figure 6. Excitation-intensity-dependent nonlinear response spectra measured for three different Si NFs. The excitation wavelengths were chosen to be (a) 804, (b) 800, and (c) 808 nm.

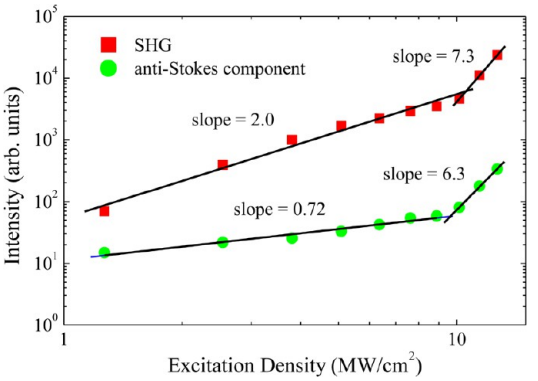

Figure 7. Excitation-intensity-dependent nonlinear signals measured for a Si NF whose nonlinear response spectra are shown in Figure 6a.

peak with strong intensity is attributed to the SHG in the Si NF because its wavelength (402 nm) is exactly half of the excitation wavelength (804 nm). We also examined the SHG by using excitation wavelengths of 780 and 760 nm, and it was found that similar SHG spectra appeared at 390 and 380 nm, respectively. An examination of the excitation-intensity-dependent signal, which is presented in Figure 7, further confirms this assignment. The fitting of the experimental data gives a slope of ∼2.0 at low excitation intensities, which is in approximately agreement with the second-order nature of the SHG. The peak with weak intensity, which is located on the short-wavelength side of the SHG, is thought to be the anti-Stokes component originating from the nonlinear Raman scattering of the Si NF. A similar phenomenon was previously observed in a Si film composed of ultrasmall Si NPs of ∼1 nm.[30] In that case, the anti-Stokes component of the Raman scattering was even

dx.doi.org/10.1021/jp408865p | J. Phys. Chem. C XXXX, XXX, XXX−XXX

stronger than the SHG. The Raman shift was estimated to be about 10 nm in our case, which is similar to that observed in ultrasmall Si NPs.[30] The line width of the Raman scattering is similar to that of the SHG, and the excitation intensity dependence of this component exhibits a slope of only 0.72 at low excitation intensities. It is noticed that a significant increase in the slope of the SHG to 7.3 was observed for excitation intensities larger than 10.16 MW/cm^2. Similarly, a rapid increase of the anti-Stokes component with a slope of 6.3 was found in the same excitation intensity regime. More experiments are needed to identify the underlying physical mechanism responsible for the rapid increase in the slopes for both the SHG and the anti-Stoke component. At present, we think that the possible mechanism is the appearance of stimulated Raman scattering because a narrowing of the line width is also observed for both the SH and the anti-Stoke component.

When we compare the spectra shown in Figures 6b and 6c, which appear to be similar, with those shown in Figure 6a, it is found that the spectra are greatly broadened with increasing excitation intensity. On both sides of the main peak which is ascribed to the SHG, one can find two shoulders which are attributed to the anti-Stokes and Stokes components of the Raman scattering of the Si NF. In this case, we need to fit the spectra with multiple Gaussian peaks to extract the anti-Stokes and Stoke shifts. The Stokes shift is derived to be 12 nm. Another noting worthy feature is the sharp cutoff of the Stokes peak at ~420 nm and the appearance of the broad luminescent band on the long-wavelength side. This feature is not observed in the spectra shown in Figure 6a. We think it is related to Si NSs with different sizes distributed in the excitation spots. For Si NSs with diameters larger than 150 nm, the scattering peak will appear in the red light or near-infrared region which is close to the excitation wavelength. In this case, it is possible generate TPL. In addition, the absorption of the SH or Raman scattering light may produce luminescence in the visible light region through single photon excitation, similar to that shown in Figure 4. However, more experiments are needed to clarify this issue.

As compared to the SHG generated by single Si NSs (see Figure 5b), the SHG generated by Si NFs is found to increase significantly after considering the increase in the number of Si NSs being excited in Si NFs. Since SHG intensity is proportional to the square of the incident light intensity,[28] the effective diameter for an excitation spot of ~1.0 μm in diameter was estimated to be 300 nm. Therefore, the number of NSs in a Si NF which contribute to SHG is estimated to be ~10. As compared to single Si NSs, however, an enhancement factor of more than 100 was found for the Si NF after considering the 10× gain used in the measurements of single Si NSs. This phenomenon can be understood by comparing the electric field distributions calculated for single Si NSs and the aggregate of Si NSs which is employed to simulate Si NFs, as discussed in the next section.

3.4. Physical Mechanism for Significantly Enhanced SHG Achieved in Si NFs. It has been shown that Si NFs exhibit a significant enhancement in SHG as compared to single Si NSs. In order to gain a deep insight into the underlying physical mechanism, we calculated numerically the electric field distributions for single Si NSs and Si aggregates by using the FDTD technique and estimated the enhancement factors for SHG. Basically, the SHG in NPs can be expressed as follows[31]

$$I_{SHG} \propto f^4(\omega) f^2(2\omega) I_{in}{}^2 \quad (1)$$

where I_{SHG} and I_{in} are the intensities of SHG and the incident light and $f(\omega)$ and $f(2\omega)$ denote the field enhancement factors at the frequencies of the fundamental light and SH, respectively. In order to compare the SHG intensities generated by Si NSs and NFs, we need to calculate the electric field distributions in them at the frequencies of the fundamental light (800 nm) and SH (400 nm). For Si NSs with diameters smaller than 100 nm, their electric field distributions appear to be similar. As a typical example, the electric field distributions for a single Si NS with a diameter of ϕ = 58 nm are shown in Figures 8a and 8b. It can

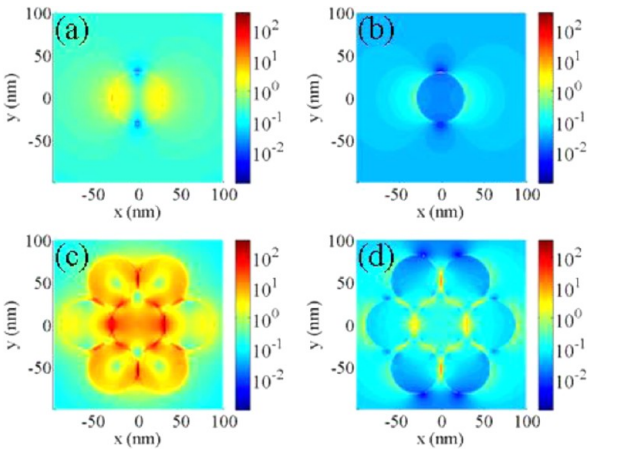

Figure 8. Electric field distributions calculated for a single Si NS with a diameter of ϕ = 58 nm and the aggregate composed of seven identical NSs arranged in a closely packed form at the fundamental light (b, d) and SH (a, c). The polarization of the incident light is along the x direction.

be seen that for both wavelengths the strongest electric field appears on the left and right surfaces of the NS where the strongest SHG signal is expected. However, it is noticed that the maximum electric field is quite weak at 800 nm because the wavelength of the incident light is much larger than the diameter of the NS. In comparison, a pronounced enhancement in electric field is observed at 400 nm which is resonant with the extinction of the NS, as shown in Figure 9. For Si NSs with diameters smaller or larger than 58 nm, the enhancement in electric field is reduced because the extinction peak does not

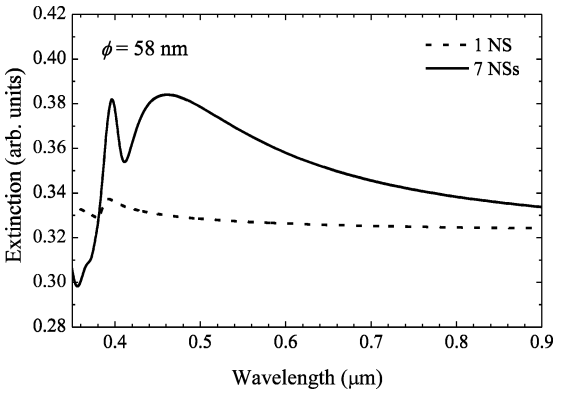

Figure 9. Extinction spectra calculated for a single Si NS with a diameter of ϕ = 58 nm and the aggregate composed of seven identical NSs arranged in a closely packed form.

dx.doi.org/10.1021/jp408865p | J. Phys. Chem. C XXXX, XXX, XXX−XXX

appear at 400 nm. For simplicity, we use an aggregate composed of seven identical NSs arranged in a closely packed form as a simple model for Si NFs. The extinction spectrum of such an aggregate is also presented in Figure 9 while the corresponding electric field distributions at 800 and 400 nm are shown in Figures 8c and 8d. It can be seen from Figure 9 that the resonant peak of the aggregate still appears at ~400 nm with a significant enhancement in extinction. Accordingly, a significant enhancement in electric field is observed for the aggregate at both the fundamental light and the SH (see Figures 8c and 8d), especially in the gap between the NSs where the centrosymmetry is broken and the contribution to the SHG is the largest. It interprets successfully the significant enhancement in the SHG observed for Si NFs in the experiments.

In order to find out the dependence of SHG intensity on the size of Si NPs, we also calculated the extinction spectra and electric field distributions for Si NSs with a larger diameter of 118 nm and the corresponding aggregate composed of seven closely packed NSs. The size of the NS is similar to the single Si NS shown in Figure 5a. For the single Si NS, it is found that the strong electric field is mainly distributed inside the NS, which is not good to SHG because of the centrosymmetry of Si. For the aggregate, however, the strong electric field in between the NSs remains nearly unchanged. Although single Si NSs with diameters larger than 100 nm are not good for strong SHG as compared to those which diameters of ~60 nm, the aggregate composed of such large NSs is expected to produce SHG with intensity similar to that composed of small NSs because of the electric field enhancement in between the NSs.

We have shown by numerical simulation that Si aggregates composed of closely packed Si NSs exhibit significant enhancement in electric field at wavelengths of both the fundamental light and the SH. Previously, the scattering spectra for the heptamers of Si and gold NSs with a larger size were investigated theoretically and numerically by Miroshnichenko et al., and Fano resonances were demonstrated.[32] It would be interesting to study the influence of the Fano resonances on the nonlinear optical properties of the heptamers if the size of the constituent Si NSs can be deliberately controlled so that the Fano resonances can be tuned to the wavelengths of the fundamental light or the SH. In practice, Si NFs are usually formed by closely packed Si NSs with different sizes, as shown in Figure 3a. In order to find out whether the enhancement in electric field is still present in such Si NFs, we have examined a typical aggregate composed of nonuniform Si NSs, as indicated by the dashed box in Figure 3a. The corresponding electric field distributions calculated at both 400 and 800 nm are presented in Figures 10a and 10b where significant enhancements in electric field with respect to single Si NSs are still present.

This simulation result is in good agreement with the experimental observation described above. It indicates that the significant enhancements in electric field originate mainly from the closely packing of Si NSs and the increased size of Si NFs as compared to single Si NSs. Since Si is a material with centrosymmetry, the SHG in Si NSs is dominated by the contribution at the surfaces where the symmetry is broken. Therefore, the narrow gap between Si NSs in Si NFs where the electric field is dramatically enhanced plays a crucial role in the achievement of significantly enhanced SHG observed in Si NFs. In contrast, the influence of the size of Si NSs on the SHG is less important because the contribution from the bulk material is negligible as compared to that of the surface material. This unique feature makes Si NFs attractive for practical application because there is no requirement for uniform Si NSs in the fabrication of Si NFs.

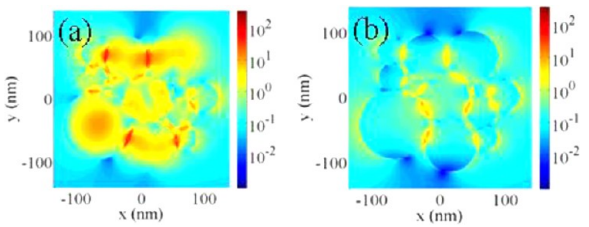

Figure 10. (a) Extinction spectra calculated for the Si aggregate composed of nonuniform Si NSs as indicated by the dashed box in Figure 3a. (b) and (c) show the electric field distributions for the aggregate at 400 and 800 nm, respectively.

4. CONCLUSION

In summary, we have investigated the assembling of Si NFs using Si NSs fabricated by fs laser ablation. The nonlinear optical responses of both single Si NSs and Si NFs were characterized by using a focused fs laser. While SHG with weak intensity was found in single Si NSs, a significant enhancement in SHG was observed in Si NFs. More importantly, the Stokes and anti-Stokes components of nonlinear Raman scattering were clearly resolved in Si NFs because of the strong SHG. The numerical simulations based on the FDTD technique reveal that the strong SHG in Si NFs originates from the strong localized electric field generated in between Si NSs that constitute Si NFs.

AUTHOR INFORMATION

Corresponding Author

*E-mail slan@scnu.edu.cn; Fax +86-20-39310309 (S.L.).

Notes

The authors declare no competing financial interest.

ACKNOWLEDGMENTS

The authors acknowledge the financial support from the National Natural Science Foundation of China (Grants 51171066 and 11374109), the Ministry of Education of China (Grant 20114407110002), and the project for high-level professionals in the universities of Guangdong province, China.

REFERENCES

(1) Pavesi, L. Will Silicon Be the Photonic Material of the Third Millenium? *J. Phys.: Condens. Matter* **2003**, *15*, R1169−1196.

(2) Soni, A.; Sundaram, V. M.; Wen, S. The Generation of Nano-Patterns on a Pure Silicon Wafer in Air and Argon with Sub-Diffraction Limit Nanosecond Laser Pulses. *J. Phys. D: Appl. Phys.* **2010**, *43*, 145301−145305.

(3) Wu, C.; Crouch, C. H.; Zhao, L.; Carey, J. E.; Younkin, R.; Levinson, J. A.; Mazur, E.; Farrell, R. M.; Gothoskar, P.; Karge, R. A. Near-Unity Below Band Gap Absorption by Microstructured Silicon. *Appl. Phys. Lett.* **2001**, *78*, 1850−1852.

(4) Wu, C.; Crouch, C. H.; Zhao, L.; Mazur, E. Visible Luminescence from Silicon Surfaces Microstructured in Air. *Appl. Phys. Lett.* **2002**, *81*, 1999−2001.

(5) Zhang, C. Y.; Yao, J. W.; Liu, H. Y.; Dai, Q. F.; Wu, L. J.; Lan, S.; Trofimov, V. A.; Lysak, T. M. Colorizing Silicon Surface with Regular Nanohole Arrays Induced by Femtosecond Laser Pulses. *Opt. Lett.* **2012**, *37*, 1106−1108.

(6) Zorba, V.; Persano, L.; Pisignano, D.; Athanassiou, A.; Stratakis, E.; Cingolani, R.; Tzanetakis, P.; Fotakis, C. Making Silicon Hydrophobic: Wettability Control by Two-Length Scales Imultaneous Patterning with Femtsecond Laser Irradiation. *Nanotechnology* **2012**, *17*, 3234−3238.
(7) Erogbogbo, F.; Yong, K. T.; Hu, R.; Law, W. C.; Ding, H.; Chang, C. W.; Prasad, P. N.; Swihart, M. T. Biocompatible Magneto-fluorescent Probes: Luminescent Silicon Quantum Dots Coupled with Superparamagnetic Iron(III) Oxide. *ACS Nano* **2010**, *14*, 5131−5138.
(8) Knipping, J.; Wiggers, H.; Rellinghaus, B.; Roth, P.; Konjhodzic, D.; Meier, C. J. Synthesis of High Purity Silicon Nanoparticles in a Low Pressure Microwave Reactor. *Nanosci. Nanotechnol.* **2004**, *4*, 1039−1044.
(9) Nayfeh, M. H.; Rao, S.; Nayfeh, O. M.; Smith, A.; Therrien, J. UV Photodetectors with Thin-Film Si Nanoparticle Active Medium. *Nanotechnology* **2005**, *4*, 660−668.
(10) Li, Z. F.; Ruckenstein, E. Water-Soluble Poly(acrylic acid) Grafted Luminescent Silicon Nanoparticles and Their Use as Fluorescent Biological Staining Labels. *Nano Lett.* **2004**, *4*, 1463−1467.
(11) Smith, A.; Yamani, Z. H.; Roberts, N.; Turner, J.; Habbal, S. R.; Granick, S.; Nayfeh, M. H. Observation of Strong Direct-Like Oscillator Strength in the Photoluminescence of Si Nanoparticles. *Phys. Rev. B* **2005**, *72*, 205307−205311.
(12) Li, X.; He, Y.; Swihart, M. T. Surface Functionalization of Silicon Nanoparticles Produced by Laser-Driven Pyrolysis of Silane Followed by HF HNO_3^- Etching. *Langmuir.* **2004**, *20*, 4720−4727.
(13) Intartaglia, R.; Bagga, K.; Scotto, M.; Diaspro, A.; Brandi, F. Luminescent Silicon Nanoparticles Prepared by Ultra Short Pulsed Laser Ablation in Liquid for Imaging Applications. *Opt. Mater. Express* **2012**, *2*, 2510−2518.
(14) Švrček, V.; Sasaki, T.; Shimizu, Y.; Koshizaki, N. Aggregation of Silicon Nanocrystals Prepared by Laser Ablation in Deionized Water. *J. Laser Micro/Nanoeng.* **2007**, *2*, 15−19.
(15) Alkis, S.; Okyay, A. K.; Ortaç, B. Post-Treatment of Silicon Nanocrystals Produced by Ultra-Short Pulsed Laser Ablation in Liquid: Toward Blue Luminescent NanoCrystal Generation. *J. Phys. Chem. C* **2012**, *116*, 3432−3436.
(16) Intartaglia, R.; Bagga, K.; Brandi, F.; Das, G.; Genovese, A.; Fabrizio, E. D.; Diaspro, A. Optical Properties of Femtosecond Laser-Synthesized Silicon Nanoparticles in Deionized Water. *J. Phys. Chem. C* **2011**, *115*, 5102−5107.
(17) Švrček, V.; Mariotti, D.; Kondo, M. Ambient-Stable Blue Luminescent Silicon Nanocrystals Prepared by Nanosecond-Pulsed Laser Ablation in Water. *Opt. Express* **2009**, *17*, 520−527.
(18) Semaltianos, N. G.; Logothetidis, S.; Perrie, W.; Romani, S.; Potter, R. J.; Edwardson, S. P.; French, P.; Sharp, M.; Dearden, G.; Watkins, K. G. J. Silicon Nanoparticles Generated by FemtoSecond Laser Ablation in a Liquid Environment. *Nanopart. Res.* **2010**, *12*, 573−580.
(19) Švrček, V.; Sasaki, T.; Katoh, R.; Shimizu, Y.; Koshizaki, N. Aging Effect Blue Luminescent Silicon Nanocrystals Prepared by Pulsed Laser Ablation of Silicon Wafer in Deionized Water. *Appl. Phys. B* **2009**, *94*, 133−139.
(20) Švrček, V.; Yamanari, T.; Shibata, Y.; Kondo, M. Tailoring of Hybrid Silicon NanoCrystal-Based Bulk Heterojunction Photovoltaic Properties upon Nanocrystal Laser Processing in Liquid Medium. *Acta Mater.* **2011**, *59*, 764−773.
(21) Kuzmin, P. G.; Shafeev, G. A.; Bukin, V. V.; Garnov, S. V.; Farcau, C.; Carles, R.; Warot-Fontrose, B.; Guieu, V.; Viau, G. Silicon Nanoparticles Produced by Femtosecond Laser Ablation in Ethanol: Size Control, Structural Characterization, and Optical Properties. *J. Phys. Chem. C* **2010**, *114*, 15266−15273.
(22) Yang, S.; Cai, W.; Zeng, H.; Li, Z. Polycrystalline Si Nanoparticles and Their Strong Aging Enhancement of Blue Photoluminescence. *J. Appl. Phys.* **2008**, *104*, 023516−023520.
(23) Intarraglia, R.; Bagga, K.; Genovese, A.; Athanassiou, A.; Cingolani, R.; Diaspro, A.; Brandi, F. Influence of Organic Solvent on Optical and Structure Properties of Ultra-Small Silicon Dots Synthesized by UV Laser Ablation in Liquid. *Phys. Chem. Chem. Phys.* **2012**, *14*, 15406−15411.
(24) Intartaglia, R.; Barchanski, A.; Bagga, K.; Genovese, A.; Das, G.; Wagener, P.; Fabrizio, E. D.; Diaspro, A.; Brandi, F.; Barcikowski, S. Bioconjugated Silicon Quantum Dots from One-Step Green Synthesis. *Nanoscale* **2012**, *4*, 1271−1274.
(25) Baggage, K.; Barchanski, A.; Intartaglia, R.; Dante, S.; Marotta, R.; Diaspro, A.; Sajti, C. L.; Brand, F. Laser-Assisted Synthesis of Staphylococcus Aureus Protein-Capped Silicon Quantum Dots as Bio-Functional Nanoprobes. *Laser Phys. Lett.* **2013**, *10*, 065603−065610.
(26) Evlyukhin, A. B.; Novikov, S. M.; Zywietz, U.; Eriksen, R. L.; Reinhardt, C.; Bozhevolnyi, S. I.; Chichkov, B. N. Demonstration of Magnetic Dipole Resonances of Dielectric Nanospheres in the Visible Region. *Nano Lett.* **2012**, *12*, 3749−3755.
(27) Fu, Y. H.; Kuznetsov, A. I.; Miroshnichenko, A. E.; Yu, Y. F.; Luk'yanchuk, B. Directional Visible Light Scattering by Silicon Nanoparticles. *Nat. Commun.* **2013**, *4*, 1527−1548.
(28) Kuznetsov, A. I.; Miroshnichenko, A. E.; Fu, Y. H.; Zhang, J. B.; Luk'yanchuk, B. Magnetic Light. *Sci. Rep.* **2012**, *2*, 492−497.
(29) Huang, C. C.; Chuang, K. Y.; Huang, C. J.; Liu, T. M.; Yeh, C. S. Graphite-Shelled Si Nanoparticles and Their Au/Si Heterodimers: Preparation, Photoluminescence, and Second Harmonic Generation. *J. Phys. Chem. C* **2011**, *115*, 9952−9960.
(30) Nayfeh, M. H.; Akcakir, O.; Belomoin, G.; Barry, N.; Therrien, J.; Gratton, E. Second Harmonic Generation in Microcrystallite Films of Ultrasmall Si Nanoparticles. *Appl. Phys. Lett.* **2000**, *77*, 4086−4088.
(31) Hubert, C.; Billot, L.; Adam, P. M.; Bachelot, R.; Royer, P.; Grand, J.; Gindre, D.; Dorkenoo, K. D.; Ford, A. Role of Surface Plasmon in Second Harmonic Generation from Gold Nanorods. *Appl. Phys. Lett.* **2007**, *90*, 181105−181107.
(32) Miroshnichenko, A.; Kivshar, Y. Fano Resonance in All-Dielectric Oligamers. *Nano Lett.* **2012**, *12*, 6459−6463.